Binary molecular design for oriented crystalline film and solution-processed interdigitated hole injection layer in quantum dot LED devices

Shota Fukuma, Wataru Sato, Akinori Takasugi, Pushi Wang, Rui Shang,* and Eiichi Nakamura*

Department of Chemistry, The University of Tokyo, 7-3-1 Hongo, Bunkyo-ku, Tokyo 113-0033, Japan
Supporting Information Placeholder

ABSTRACT: Printable electronics typically employ amorphous materials for layer uniformity, yet incorporating crystalline substances can significantly enhance device performance due to their superior carrier mobility. The implementation of interdigitated structures facilitates increased carrier injection and extraction while reducing transport paths, thus elevating device efficiency. This research addresses the challenges associated with the molecular design, assembly, and orientation control of crystalline structures on indium tin oxide substrates, focusing on augmenting hole injection and transport efficiency. We introduce a binary molecular design involving benzodipyrrole diesters (BDPCOs), where two polar-orienting ester groups are incorporated into an aromatic BDP core. Our findings reveal that the ester moiety's structure substantially influences film formation, with certain BDPCOs yielding highly crystalline films, whereas others result in oriented, non-crystalline films. Perovskite quantum dot (PVQD) LEDs incorporating a crystalline BDPCO-based hole injection layer (HIL) exhibit superior luminescence compared to devices utilizing amorphous BDPCO or PEDOT:PSS HILs. This binary molecular design approach thus broadens the range of solution-processible crystalline films for advanced electronic device applications.

The fabrication of printable electronics principally involves creating layered structures through the precision printing of electronic components, focusing on electron and hole transfer management between the cathode and anode (Figure 1a).[1-7] A prevalent method for enhancing efficiency utilizes amorphous materials, which may be completely random[8] or partially ordered[9-13], to guarantee uniform layers with consistent thickness. However, crystalline materials, known for their superior carrier mobility compared to their amorphous organic counterparts,[14-17] have been recognized for their potential to significantly

improve device performance.[18-25] Moreover, these crystalline substances can enable the formation of interdigitated structures, which offer several advantages. These include enhanced carrier separation and recombination, optimized carrier injection and extraction, and reduced carrier transport paths, all contributing to the overall efficiency of the device.[26-27] This benefit of crystalline materials has previously been evidenced in the active layers of organic solar cell devices (Figure 1b).[28]
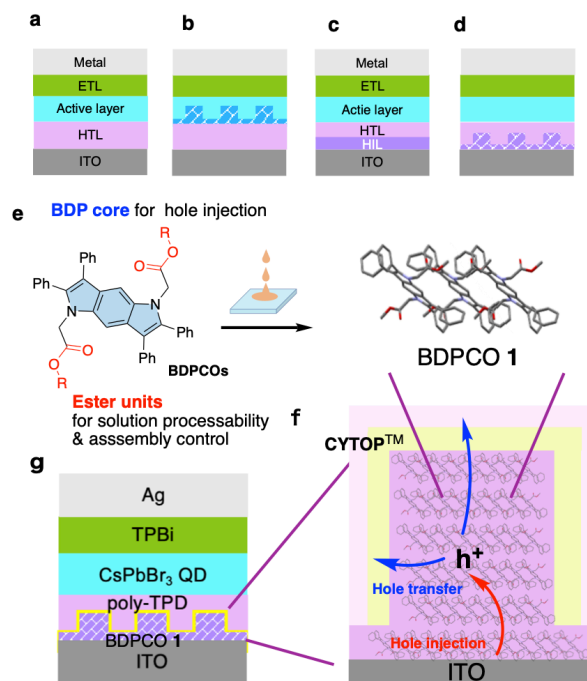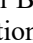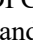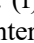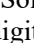

Figure 1. Concept and design of solution-processable ordered hole injection layers for PVQD-LED devices and device configuration in our study. (a) Organic optoelectronic devices based on flat layers. (b) Interdigitation in the active layer. (c) Typical devices based on bilayered hole transporter. (d) Interdigitation in the hole injection

layer. (e) Binary molecular design in BDPCO. (f) Solution processable oriented crystallization and interdigitation for LED devices. (g) The PVQD-LED device architecture using interdigitated hole injection layer.

Despite the benefits, the execution of multi-layered structures (Figure 1c) presents scientific and practical challenges, particularly in molecular design, assembly, and orientation control on indium tin oxide (ITO) substrates[29]. This study focuses on supramolecular strategy, design of crystalline interdigitated layer to enhance the efficiency of hole injection from the cathode and its transport to the HTL (Figure 1d). We propose a binary molecular design of benzodipyrrole diesters (BDPCOs), integrating two polar-orienting ester groups into an aromatic BDP core (Figure 1e). We demonstrate the formation of a highly uniaxially oriented film via solution-driven crystal growth (Figure 1f), and its application to a hole injection layer (HIL) in solution-processed perovskite quantum dot light emitting diodes (PVQD-LEDs) (Figure 1g), which are garnering attention as next-generation LEDs.[30-34]

We examined fourteen BDPCO derivatives and chose compounds **1**–**6** for detailed studies considering the solubility and crystal-formation ability required for this study (Figure 2). They were first spin-coated and thermally annealed on an ITO substrate, revealing that their film structure depends on the structure of the ester moiety. For example, spin-coating of a chlorobenzene solution of a derivative **1** on ITO undergoes 2D-layer stacking through interaction of the aromatic ring and the diester groups, forming a film made of crystalline stacks (Figures 1e). In contrast, derivative **4**, possessing racemic 2-butyl groups, forms an oriented, yet non-crystalline film. Grazing-Incidence wide-angle X-ray scattering (GIWAXS) measurements on the film of **1**, juxtaposed with its single-crystal packing, confirmed a uniaxial orientation on the ITO substrate (Figure 1g). Similar uniaxial orientation structures were also observed in other derivatives such as **2**, **5**, and **6**. We investigated their performance as HIL for PVQD-LEDs (Figure 1f), where we coated a few-nm thick fluorous film of CYTOP(TM) between the HIL of BDPCO **1** and a hole-transporting layer (HTL) of amorphous poly-TPD (poly[*N,N*'-bis(4-butylphenyl)-N,N'-bis(phenyl)-benzidine) to increase reproducibility.[35-36] Notably, the device using a crystalline film of BDPCO derivative **1** as the HIL, displaying green luminescence (maximum of 4526 cd/m² among several runs, FWHM = 25 nm), outperformed both the device made from its amorphous counterpart and the reference device (2008 cd/m²) using amorphous PEDOT:PSS (cf. Figure 1a). This underscores the superior hole injection/transfer abilities of crystalline HILs from ITO to HTL. These findings illustrate that a suitable binary molecular design can facilitate the formation of highly oriented crystals on an ITO substrate, thereby achieving efficient hole injection and transport.
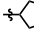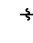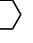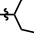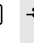
Figure 2. Fifteen BDPCO derivatives synthesized and their basic characterizations. The check-marked compounds were examined in detail, which cross-marked ones were not.

RESULTS AND DISCUSSION

Synthesis and Characterization of BDPCOs. BDPCOs were synthesized in two steps. First, the 2,3,6,7-tetraphenylbenzo[1,2-b:4,5-b′]dipyrrole core (BDP) was produced on a 20-gram scale using a well-established coupling reaction between *p*-phenylenediamine and benzoin.[37] Note that various other derivatives are available by the use of synthetic methods that we reported recently.[38-39] Subsequently, an S_N2 reaction was conducted with alkyl-bromoacetate to introduce ester groups on the nitrogen atoms (Figure 3a). Employing various alkyl bromoacetates, we prepared BDPCO derivatives with a total of 14 variants. This includes linear alkyl groups ranging from methyl to butyl, branched alkyl groups such as 2-buthyl, and cycloalkyl groups from cyclopentyl to cyclooctyl, and 1-adamantyl groups. More than half of these compounds afforded X-ray quality single crystals, and molecules **1**-**6**, which formed a characteristic ordered structure on ITO as revealed by GIWAXS analysis, were further studied for their performance as HIL in QD LED devices. The butyl ester **7** and the cycloheptyl ester **12** showed the same crystal packing structure as propyl **3** and cyclooctyl esters **6**, respectively, and hence were not studied further (see chapter 2 of the SI).
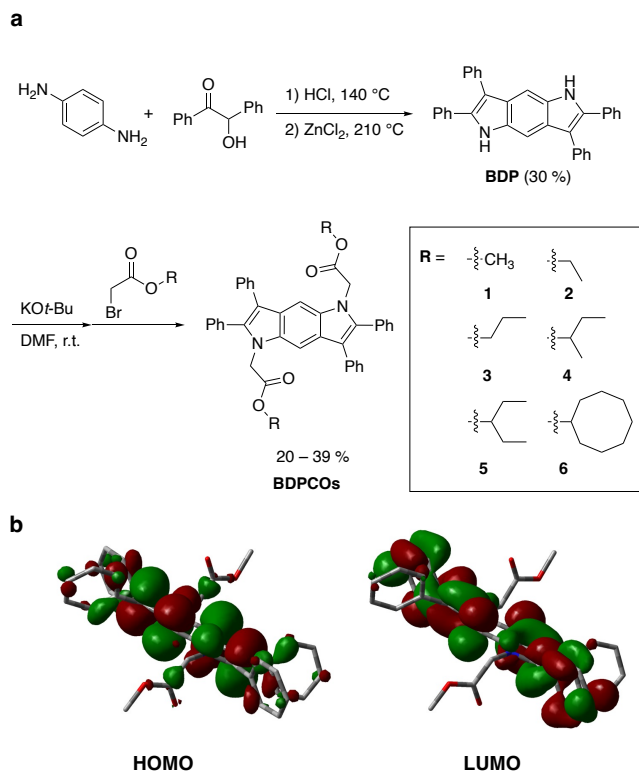
Figure 3. Synthesis and structures of BDPCOs. (a) Synthesis of BDPCOs. (b) HOMO and LUMO of BDPCO **1** determined at the B3LYP/6-31G(d) level.

The HOMO and LUMO of BDPCO 1 are fully delocalized over the entire BDP core (Figure 3b), with HOMO level of **1** determined by photoelectron yield spectroscopy (PYS) lies 5.40 eV. The photoemission and absorption spectra of **1** in CH_2Cl_2 showed an emission peak at 410 nm and a bandgap of 3.4 eV (Figure S17). Differing only for the ester groups, all compounds show largely the same frontier orbital properties as indicated by DFT calculations, which are shown in the Supporting Information (Figure S12). The HOMO and band gap data suggest that the choice of the ester group negligibly affects the BDPCO core's electronic properties, while significantly impacts molecular packing in the crystal and subsequent HIL performance as discussed below. These molecule-level properties parallel those of previously studied congeners, which bear two racemic alkyl sulfonate side chains replacing the ester side chains of BDPCO, and create an efficient amorphous HTL for perovskite solar cell devices.[40-41]

BDPCOs **1**–**6** show adequate solubility as spin-coated on ITO with halogen-containing organic solvents such as dichloroethane, chloroform, and chlorobenzene (Figure S15), the parent BDP compound without ester units do not, highlighting the ester groups' critical role in improving device processability. All BDPCOs proved thermally stable up to 200°C, as confirmed by thermogravimetric analysis (see Figure S18).

Assembly Characteristics in the BDPCO Thin Films.
To decipher the crystal orientations on the ITO substrate, we simulated the GIWAXS diffraction patterns of the uniaxially oriented crystalline film using the single-crystal X-ray structures of the BDPCOs. The GIWAXS images of **1**,**2**,**5**, and **6** (Figure 4) showed several well-defined diffraction spots, indicative of ordered assembly with anisotropic molecular packing on the ITO plane, suggesting that the film consists of crystalline molecules with a single specific orientation. Thus, we deciphered the orientations of molecular assembly in the crystalline thin films of BDPCOs **1**, **5**, and **6** as presented in Figures 4a, b, and c. High resolution 2θ-θ XRD data is also employed to determination of orientation of nearly-cubic **5** (Figure S16). Although the ethyl ester derivative (BDPCO **2**) formed a uniaxially oriented film as indicated from the GIWAXS data (Figure 4k), it did not align with the sole single crystal packing structure we obtained (Figure 4j). Given the discovery of two polymorphs isolated by recrystallization of the propyl ester (BDPCO **3**), it is plausible that the polymorph of the ethyl ester **2** grown on the ITO substrate differs from the one obtained via solution-phase recrystallization.
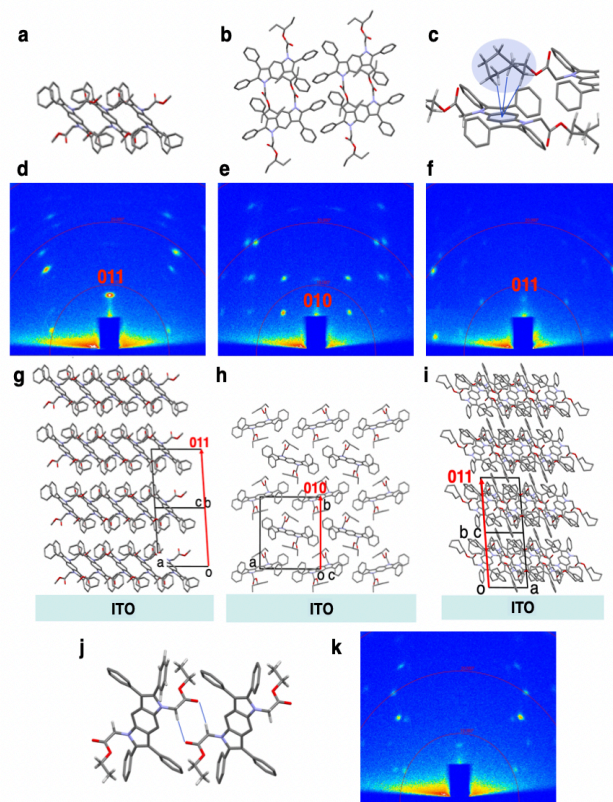

Figure 4. X-ray analyses of crystalline BDPCOs. Crystal packing structures of (a) **1** (b) **5** (c) **6** (j) **2**. GIWAXS analysis of BDPCO films (d) **1** (e) **5** (f) **6** spin-coated onto ITO substrates. Structure of the molecular assembly of (g) **1**, (h) **5**, (i) **6** in the film state determined by X-ray analyses

Notably, BDPCOs **1**, **2**, **5**, and **6** displayed distinct crystallization manners—**1** as slip-stack, **2** as face-to-edge herringbone arrangement, and **5** and **6** forming face-to-face herringbone structures. Each compound, in particular, **1**, **5**, and **6** exhibited unique assembly patterns on the ITO substrate. The crystal packing of the cyclooctyl ester (BDPCO **6**) is particularly noteworthy, where the BDP core is flanked by CH/π-interactions (indicated by blue lines) with two cyclooctyl groups from adjacent BDPCO molecules. This configuration effectively prevents the BDP core from directly interacting with neighboring π-systems, thereby inhibiting unwanted aggregation and precipitation. Despite the varying crystal packing and local environments of the BDP π-systems, QD-LED devices incorporating BDPCOs **1**, **2**, **5**, and **6** consistently outperformed those using less oriented crystals of BDP-COs **3** and **4**, with the results and implications of this observed in subsequent device performance analyses.
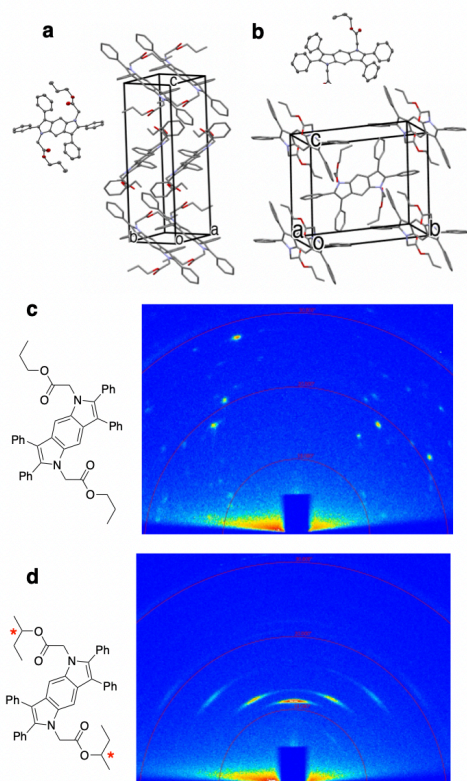

Figure 5. Crystallographic and film-state analysis of **3** and **4**. (a) (b) Crystal structures of the two polymorphs of **3**. Single-molecular structures are shown with Oak Ridge thermal ellipsoid plot (ORTEP) drawing with thermal ellipsoids set to 50% probability. Hydrogen atoms are omitted for clarity. (c) GIWAXS analysis of **3**. (d) GIWAXS analysis of **4**.

In all films studied, a recurring theme in molecular assembly was noted, where the π-planes align within the plane of the 2D molecular structure, facilitated by ester units. This orientation enhances in-plane interactions

through electrostatic dipole and/or π-stacking interactions (Figure 4 g-i). In contrast, the interactions occurring out-of-plane among these 2D molecular assemblies involved comparatively weaker CH-π interactions between the benzene rings encircling the BDP core (**1** and **6**) or alkyl groups at ester units (**5**). This observation indicates that the spontaneous self-assembly of BDPCOs is predominantly influenced by a hierarchical sequence of stacking interactions.
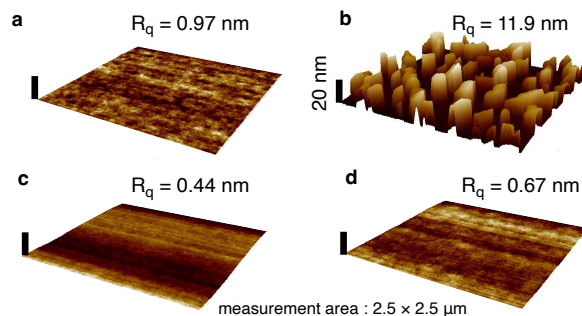

Figure 6. AFM images of spin-coated compound **1**. (a) As spin-coated using chlorobenzene solution. (b) After thermal annealing at 130 °C. (c) As spin-coated using chloroform solution. (d) After thermal annealing at 60 °C.

Atomic Force Microscopy (AFM) analysis of the film of BDPCO **1** revealed that the films comprise crystals measuring 20–30 nm in thickness and approximately 100 nm in width, indicating larger in-plane dimensions and smaller out-of-plane dimensions (Figure 4). This structural aspect suggests that the horizontal alignment of the stronger interactions between ester units, combined with the vertical arrangement of the weaker CH-π interactions, serves to minimize the overall energy within the crystal. Consequently, this arrangement facilitates enhanced hole injection from the ITO substrate and efficient hole transfer to the HTL through the interdigitated HIL/HTL interface (Figure 1g). Moreover, the in-plane interactions include two-fold hydrogen bonds, with a bond length of 2.36Å, between adjacent ester units in BDPCO **2**, and three-fold CH-π interactions in BDPCO **6**. These interactions occur between the two cyclooctyl groups and the central benzene ring of the BDP core, contributing further to the observed molecular assembly and device performance, as above discussed. In contrast to other BDPCOs, the GIWAXS pattern of BDPCO **3** featured numerous asymmetrically distributed circular spots, as seen in Figure 5c. This pattern suggests the simultaneous growth of two different polymorphs, a hypothesis that was confirmed when recrystallization from a CH_2Cl_2/EtOAc solution resulted in the concurrent formation of two polymorphs. This phenomenon is attributed to C–C bond rotational isomers in the propyl chains, as illustrated in Figures 5a and b. BDPCO **4**, on the other hand, exhibited a unique behavior. Its GIWAXS image showed crescent-shaped patterns (Figure 5d), indicative of local molecular disorder. This disorder is believed to be caused by the ra-

cemic 2-butyl side chains, which lead to a 1:1 diastereomeric mixture that interferes with crystallization. Attempts to crystallize BDPCO **4** using a CH_2Cl_2/EtOAc bilayer system, a method that typically facilitates the formation of large crystals (over 200 μm) in other BDPCO derivatives, were unsuccessful. This indicates the notably low crystallinity of BDPCO **4**. Conclusively, the molecular assembly observed in the film state can be effectively modulated by alterations to the alkyl chains of the ester groups. These modifications directly influence the preferred packing geometry and types of intermolecular interactions, which in turn have significant implications for the performance of LED devices. These findings and their impact on device performance will be further explored in the subsequent sections.

PVQD-LEDs using BDPCO as HIL. The structural characteristics and crystallinity of BDPCO diesters on ITO surfaces are considerably affected by the specific ester group attached. As described above, the presence of propyl groups in BDPCO **3** and racemic 2-butyl groups in BDPCO **4** hinders the formation of oriented crystals on the ITO substrate. However, the impact of these ester groups on the molecular level properties of the BDPCO molecules, the photophysical properties and molecular orbitals (MO), is minimal. Given these findings, we were compelled to investigate the correlation between crystal packing in BDPCOs and the performance of LEDs where BDPCOs serve as HILs. We posited that well-ordered crystal structures would facilitate enhanced hole injection due to their clearly defined pathways for charge carriers, as illustrated in Figure 1g. Additionally, the rough surface texture of the film, as revealed by AFM analysis, was anticipated to create an efficient interdigitated interface with the HTL coated over the HIL. This interface is expected to further improve the overall performance of the LEDs.

To validate our hypotheses, we incorporated BDPCOs into a PVQD-LED device. These devices present several benefits compared to their organic LED counterparts, notably in terms of superior brightness, dynamic range, and color purity. Additionally, PVQD-LEDs hold a potential advantage over chalcogenide-based QD LEDs due to their compatibility with low-temperature, solution-processed QD synthesis. This compatibility makes PVQD-LEDs a promising candidate for the efficient and scalable production of high-performance devices.[42-43]

To validate our hypotheses, we incorporated BDPCOs into a PVQD-LED device. These devices present several benefits compared to their organic LED counterparts, notably in terms of superior brightness, dynamic range, and color purity. Additionally, PVQD-LEDs hold a potential advantage over chalcogenide-based QD LEDs due to their compatibility with low-temperature, solution-processed QD synthesis. This compatibility makes PVQD-LEDs a promising candidate for the efficient and scalable production of high-performance devices.[42-43]

Leveraging these process advantages, our objective was to develop highly luminous PVQD-LED devices. In the forthcoming sections, we will delve into the detailed architecture of these devices and the performance outcomes of PVQD-LEDs that utilize BDPCOs as HIL. This discussion will provide insight into the effectiveness of BDPCOs in enhancing device performance and their potential implications for future LED technology developments.

For our investigation, we chose green-emitting PVQD-LED devices (Figure 7b) with a well-established device architecture: ITO/HIL (25~35 nm)/poly-TPD (25 nm)/$CsPbBr_3$ green QD (40 nm)/TPBi (30 nm)/Ag (100 nm) (Figure 7a).[1] Commercially available QD powder from Quantum Solutions Co. was used for this study. To set a benchmark, we used a standard HIL material, PEDOT:PSS,[44-45] and compared the performance of BDPCO thin films against it. In devices with only poly-TPD and no HIL, we observed a luminance of 826 ± 155 cd/m^2. Devices with PEDOT:PSS as the HIL and poly-TPD as the HTL showed a luminance of 2008 ± 156 cd/m^2. The PVQD-LEDs used in this work all showed sharp green electroluminescence (515 nm) with FWHM of 25 nm.
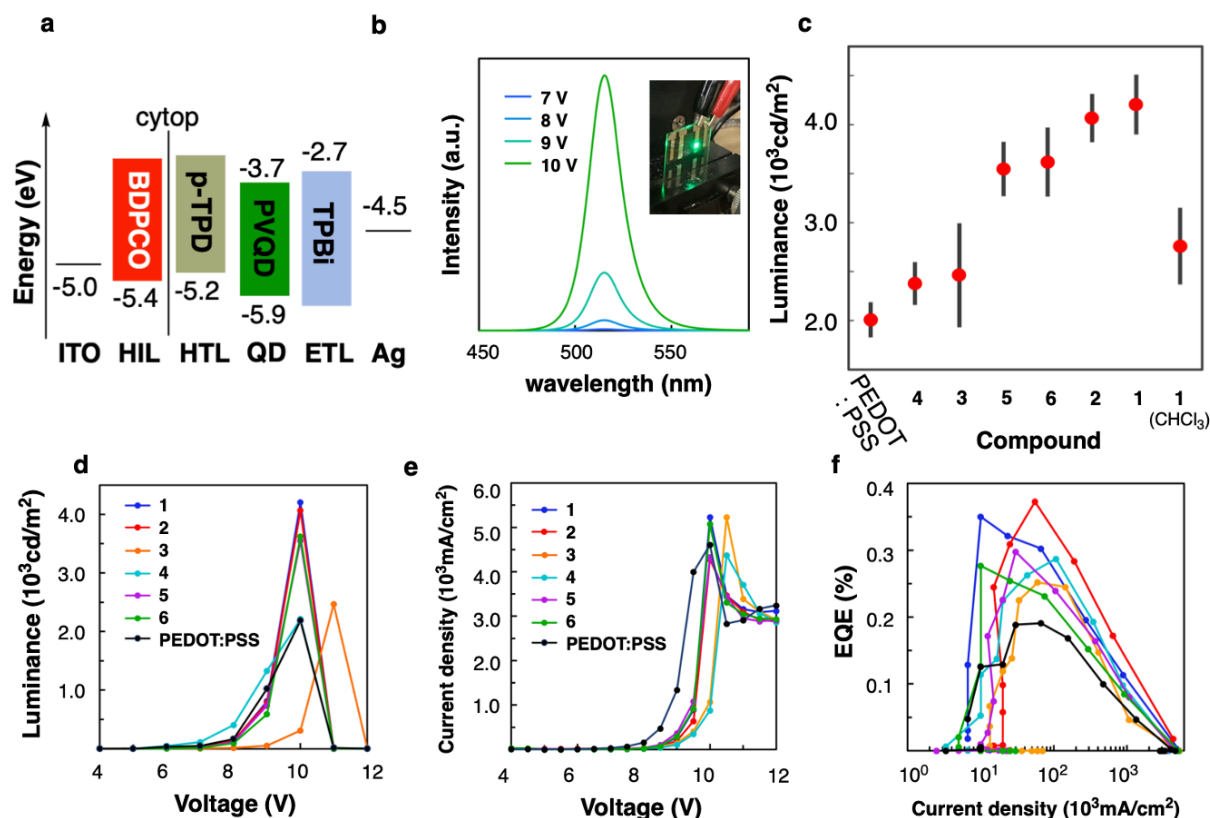
Figure 7. Investigation of PVQD-LED devices. (a) Energy level alignment of the PVQD-LED devices in this study. (b) The electroluminescent spectrum of a PVQD-LED device using **1**. (c) Maximum luminance (d) L-V curves (e) J-V curves (f) EQE of the devices using different HIL. The BDPCO films were spin-coated from chlorobenzene solution except specifically noted in the parentheses.

We formed the HIL/HTL layer in three stage (Figure 1g) first by spin-coating a chlorobenzene solution of BDPCO followed by annealing at 130 °C. We then coated a thin CYTOP layer on the HIL to reduce the standard deviation of the luminance values. Our previous reports indicated that CYTOP as thin as 1 nm thickness can stabilize the nano interface without affecting the device performance,[46-47] the fact that has been corroborated by various studies since then,[48-49] and the onset voltage observed for all BDPCO examined was approximately 6.5 V. The impact of incorporating BDPCO as the HIL on the PVQD-LED device performance will be discussed in the next section. The devices using a crystalline film of BDPCO/poly-TPD as the hole injection layer demonstrated uniformly better performance than the one using amorphous HIL. The devices using crystalline BDPCOs **1** showed the highest luminance, reaching 4205 ± 285 cd/m^2, and those using **2** showed a comparable luminance, reaching 4067 ± 226 cd/m^2. These values are approximately twice as high as those achieved by the device using PEDOT-PSS/poly-TPD (2008 cd/m^2). The luminance data recorded for crystalline films of BDPCOs **5** and **6** were slightly lower, at 3548 ± 258 cd/m^2 and 3620

$\pm$ 332 cd/m^2, respectively, possibly suggesting the adverse effects of insulating alkyl groups in these compounds.

CONCLUSION

Our research introduces a binary molecular design, integrating a planar benzodipyrrole (BDP) core with two strategically selected ester groups, each adorned with suitable alkyl chains. This innovative design facilitated the successful development of bright PVQD-LEDs using orderly crystalline films of BDP core-ester compounds as HILs. Our comprehensive analysis highlighted that the specific structure of the ester group profoundly influences the film morphology. Certain derivatives yielded highly crystalline films, while others resulted in films that were oriented yet non-crystalline or even amorphous. Notably, PVQD-LEDs equipped with a crystalline BDPCO-based HIL demonstrated superior luminescence when compared to reference devices employing amorphous BDPCO or PEDOT: PSS as the HIL. These findings underscore the inherent advantages of crystalline materials over their amorphous counterparts and indicate that these benefits can be effectively leveraged through the meticulous de-

sign of solution-processable organic materials. Our binary molecular design strategy offers a versatile approach to this end, paving the way for the advancement of innovative materials tailored for electronic device applications.

ASSOCIATED CONTENT

Supporting Information. Materials, methods, and supporting figures are available free of charge via the Internet at http://pubs.acs.org.

AUTHOR INFORMATION

Corresponding Author

rui@chem.s.u-tokyo.ac.jp (R.S.)
nakamura@chem.s.u-tokyo.ac.jp (E.N.)

REFERENCES

(1) Hains, A. W.; Liang, Z.; Woodhouse, M. A.; Gregg, B. A. Molecular Semiconductors in Organic Photovoltaic Cells. *Chem. Rev.* **2010**, *110*, 6689–6735.

(2) Inganäs, O. Organic Photovoltaics over Three Decades. *Adv. Mater.* **2018**, *30*, 1800388.

(3) Mitschke, U.; Bäuerle, P. The electroluminescence of organic materials. *J. Mater. Chem.* **2000**, *10*, 1471–1507.

(4) Wong, M. Y.; Zysman-Colman, E. Purely Organic Thermally Activated Delayed Fluorescence Materials for Organic Light-Emitting Diodes. *Adv. Mater.* **2017**, *29*, 1605444

(5) Huang, T.; Jiang, W.; Duan, L. Recent progress in solution processable TADF materials for organic light-emitting diodes. *J. Mater. Chem. C* **2018**, *6*, 5577–5596.

(6) Jung, H. S.; Park, N.-G. Perovskite Solar Cells: From Materials to Devices. *Small* **2015**, *11*, 10–25.

(7) Kim, J. Y.; Lee, J.-W.; Jung, H. S.; Shin, H.; Park, N.-G. High-Efficiency Perovskite Solar Cells. *Chemical Reviews* **2020**, *120*, 7867–7918.

(8) Shirota, Y.; Kageyama, H. Charge Carrier Transporting Molecular Materials and Their Applications in Devices. *Chem. Rev.* **2007**, *107*, 953-1010.

(9) Watanabe, Y.; Sasabe, H.; Kido, J. Review of Molecular Engineering for Horizontal Molecular Orientation in Organic Light-Emitting Devices. *Bull. Chem. Soc. Jpn.* **2019**, *92*, 716–728.

(10) Yokoyama, D.; Sakaguchi, A.; Suzuki, M.; Adachi, C. Horizontal molecular orientation in vacuum-deposited organic amorphous films of hole and electron transport materials. *Appl. Phys. Lett.* **2008**, *93*, 173302.

(11) Shibata, M.; Sakai, Y.; Yokoyama, D. Advantages and disadvantages of vacuum-deposited and spin-coated amorphous organic semiconductor films for organic light-emitting diodes. *J. Mater. Chem. C* **2015**, *3*, 11178–11191.

(12) Kim, J. Y.; Yokoyama, D.; Adachi, C. Horizontal Orientation of Disk-like Hole Transport Molecules and Their Application for Organic Light-Emitting Diodes Requiring a Lower Driving Voltage. *J. Phys. Chem. C* **2012**, *116*, 8699–8706.

(13) Kim, J. Y.; Yasuda, T.; Yang, Y. S.; Adachi, C. Bifunctional Star-Burst Amorphous Molecular Materials for OLEDs: Achieving Highly Efficient Solid-State Luminescence and Carrier Transport Induced by Spontaneous Molecular Orientation. *Adv. Mater.* **2013**, *25*, 2666–2671.

(14) Wang, C.; Dong, H.; Jiang, L.; Hu, W. Organic semiconductor crystals. *Chem. Soc. Rev.* **2018**, *47*, 422-500.

(15) O'Neill, M.; Kelly, S. M. Ordered Materials for Organic Electronics and Photonics. *Adv. Mater.* **2011**, *23*, 566–584.

(16) Lee, J. Y.; Roth, S.; Park, Y. W. Anisotropic field effect mobility in single crystal pentacene. *Appl. Phys. Lett.* **2006**, *88*, 252106.

(17) Sundar, V. C.; Zaumseil, J.; Podzorov, V.; Menard, E.; Willett, R. L.; Someya, T.; Gershenson, M. E.; Rogers, J. A. Elastomeric Transistor Stamps: Reversible Probing of Charge Transport in Organic Crystals. *Science* **2004**, *303*, 1644–1646.

(18) Nakanotani, H.; Adachi, C. Organic light-emitting diodes containing multilayers of organic single crystals. *Appl. Phys. Lett.* **2010**, *96*, 053301.

(19) Horowitz, G. Organic Field-Effect Transistors. *Adv. Mater.* **1998**, *10*, 365–377.

(20) Pisula, W.; Zorn, M.; Chang, J. Y.; Müllen, K.; Zentel, R. Liquid Crystalline Ordering and Charge Transport in Semiconducting Materials. *Macromol. Rapid Commun.* **2009**, *30*, 1179–1202.

(21) Larik, F. A.; Faisal, M.; Saeed, A.; Abbas, Q.; Kazi, M. A.; Abbas, N.; Thebo, A. A.; Khan, D. M.; Channar, P. A. Thiophene-based molecular and polymeric semiconductors for organic field effect transistors and organic thin film transistors. *J. Mater. Sci.: Mater. Electron.* **2018**, *29*, 17975–18010.

(22) Liu, C.-F.; Liu, X.; Lai, W.-Y.; Huang, W. Organic Light-Emitting Field-Effect Transistors: Device Geometries and Fabrication Techniques. *Adv. Mater.* **2018**, *30*, 1802466.

(23) Wan, Y.; Deng, J.; Wu, W.; Zhou, J.; Niu, Q.; Li, H.; Yu, H.; Gu, C.; Ma, Y. Efficient Organic Light-Emitting Transistors Based on High-Quality Ambipolar Single Crystals. *ACS Appl. Mater. Interfaces* **2020**, *12*, 43976–43983.

(24) Jiang, Y.; Liu, Y.-Y.; Liu, X.; Lin, H.; Gao, K.; Lai, W.-Y.; Huang, W. Organic solid-state lasers: a materials view and future development. *Chem. Soc. Rev.* **2020**, *49*, 5885–5944.

(25) Zhang, X.; Dong, H.; Hu, W. Organic Semiconductor Single Crystals for Electronics and Photonics. *Adv. Mater.* **2018**, *30*, 1801048.

(26) Huang, D.; Xiang, H.; Ran, R.; Wang, W.; Zhou, W.; Shao, Z. Recent Advances in Nanostructured Inorganic Hole-Transporting Materials for Perovskite Solar Cells. *Nanomaterials* **2022**, *12*, 2592.

(27) Liu, H.; Huang, Z.; Wei, S.; Zheng, L.; Xiao, L.; Gong, Q. Nanostructured electron transporting materials for perovskite solar cells. *Nanoscale* **2016**, *8*, 6209–6221.

(28) Matsuo, Y.; Sato, Y.; Niinomi, T.; Soga, I.; Tanaka, H.; Nakamura, E. Columnar structure in bulk heterojunction in solution-processable three-layered pin organic photovoltaic devices using tetrabenzoporphyrin precursor and silylmethyl [60] fullerene. *J. Am. Chem. Soc.* **2009**, *131*, 16048–16050.

(29) Yokoyama, D. Molecular orientation in small-molecule organic light-emitting diodes. *J. Mater. Chem.* **2011**, *21*, 19187–19202.

(30) Li, Y.-F.; Feng, J.; Sun, H.-B. Perovskite quantum dots for light-emitting devices. *Nanoscale* **2019**, *11*, 19119–19139.

(31) Dong, Y.; Wang, Y.-K.; Yuan, F.; Johnston, A.; Liu, Y.; Ma, D.; Choi, M.-J.; Chen, B.; Chekini, M.; Baek, S.-W.; et al. Bipolar-shell

resurfacing for blue LEDs based on strongly confined perovskite quantum dots. *Nat. Nanotechnol.* **2020**, *15*, 668–674.

(32) Wang, H. C.; Bao, Z.; Tsai, H. Y.; Tang, A. C.; Liu, R. S. Perovskite quantum dots and their application in light-emitting diodes. *Small* **2018**, *14*, 1702433.

(33) Chiba, T.; Kido, J. Lead halide perovskite quantum dots for light-emitting devices. *J. Mater. Chem. C* **2018**, *6*, 11868–11877.

(34) Chevalier, O. J. G. L.; Nakamuro, T.; Sato, W.; Miyashita, S.; Chiba, T.; Kido, J.; Shang, R.; Nakamura, E. Precision Synthesis and Atomistic Analysis of Deep-Blue Cubic Quantum Dots Made via Self-Organization. *J. Am. Chem. Soc.* **2022**, *144*, 21146–21156.

(35) Guo, Y.; Liu, C.; Tanaka, H.; Nakamura, E. Air-stable and solution-processable perovskite photodetectors for solar-blind UV and visible light. *J. Phys. Chem. Lett.* **2015**, *6*, 535–539.

(36) Tanaka, H.; Abe, Y.; Matsuo, Y.; Kawai, J.; Soga, I.; Sato, Y.; Nakamura, E. An Amorphous Mesophase Generated by Thermal Annealing for High-Performance Organic Photovoltaic Devices. *Adv. Mater.* **2012**, *24*, 3521–3525.

(37) Kinsley, D. A.; Plant, S. G. P. 1. The synthesis and structure of some pyrroloindoles. *J. Chem. Soc.* **1958**, 1–7.

(38) Tsuji, H.; Yokoi, Y.; Furukawa, S.; Nakamura, E. Hexaaryl-benzodipyrroles: properties and application as amorphous carrier-transporting materials. *Heterocycles* **2015**, *90*, 261–270.

(39) Tsuji, H.; Yokoi, Y.; Mitsui, C.; Ilies, L.; Sato, Y.; Nakamura, E. Tetraaryl-Substituted Benzo [1, 2-b: 4, 5-b′] dipyrroles: Synthesis, Properties, and Applications to Hole-Injection Materials in OLED Devices. *Chem. - Asian J.* **2009**, *4*, 655–657.

(40) Shang, R.; Zhou, Z.; Nishioka, H.; Halim, H.; Furukawa, S.; Takei, I.; Ninomiya, N.; Nakamura, E. Disodium Benzodipyrrole Sulfonate as Neutral Hole-Transporting Materials for Perovskite Solar Cells. *J. Am. Chem. Soc.* **2018**, *140*, 5018–5022.

(41) Zhou, Z.; Qiang, Z.; Sakamaki, T.; Takei, I.; Shang, R.; Nakamura, E. Organic/inorganic hybrid *p*-type semiconductor doping affords hole transporting layer free thin-film perovskite solar cells with high stability. *ACS Appl. Mater. Interfaces* **2019**, *11*, 22603–22611.

(42) Li, J.; Xu, L.; Wang, T.; Song, J.; Chen, J.; Xue, J.; Dong, Y.; Cai, B.; Shan, Q.; Han, B. 50-Fold EQE improvement up to 6.27% of solution-processed all-inorganic perovskite CsPbBr3 QLEDs via surface ligand density control. *Adv. Mater.* **2017**, *29*, 1603885.

(43) Liu, P.; Chen, W.; Wang, W.; Xu, B.; Wu, D.; Hao, J.; Cao, W.; Fang, F.; Li, Y.; Zeng, Y. Halide-rich synthesized cesium lead bromide

perovskite nanocrystals for light-emitting diodes with improved performance. *Chem. Mater.* **2017**, *29*, 5168–5173.

(44) Sun, K.; Zhang, S.; Li, P.; Xia, Y.; Zhang, X.; Du, D.; Isikgor, F. H.; Ouyang, J. Review on application of PEDOTs and PEDOT: PSS in energy conversion and storage devices. *J. Mater. Sci.: Mater. Electron.* **2015**, *26*, 4438–4462.

(45) Groenendaal, L.; Jonas, F.; Freitag, D.; Pielartzik, H.; Reynolds, J. R. Poly (3, 4-ethylenedioxythiophene) and its derivatives: past, present, and future. *Adv. Mater.* **2000**, *12*, 481–494.

(46) Guo, Y.; Shoyama, K.; Sato, W.; Nakamura, E. Polymer stabilization of lead (II) perovskite cubic nanocrystals for semitransparent solar cells. *Adv. Energy Mater.* **2016**, *6*, 1502317.

(47) Yang, F.; Chen, H.; Zhang, R.; Liu, X.; Zhang, W.; Zhang, J.; Gao, F.; Wang, L. Efficient and spectrally stable blue perovskite light-emitting diodes based on potassium passivated nanocrystals. *Adv. Funct. Mater.* **2020**, *30*, 1908760.

(48) Zheng, Y.; Shi, W.; Kong, J.; Huang, D.; Katz, H. E.; Yu, J.; Taylor, A. D. A cytop insulating tunneling layer for efficient perovskite solar cells. *Small Methods* **2017**, 1700244.

(49) Sun, J.; Wu, J.; Tong, X.; Lin, F.; Wang, Y.; Wang, Z. M. Organic/inorganic metal halide perovskite optoelectronic devices beyond solar cells. *Adv. Science* **2018**, *5*, 1700780.

TOC